Solar Energy Materials & Solar Cells 95 (2011) 2805–2810

Contents lists available at ScienceDirect

Solar Energy Materials & Solar Cells

journal homepage: www.elsevier.com/locate/solmat

Influence of deep level defects on the performance of crystalline silicon solar cells: Experimental and simulation study

Adnan Ali [a], Terence Gouveas [b], M.-A. Hasan [b], Saleem H. Zaidi [c], Muhammad Asghar [a,*]

[a] Semiconductor Physics Laboratory, Department of Physics, The Islamia University of Bahawalpur, Pakistan
[b] Department of Electrical and Computer Engineering, University of North Carolina, Charlotte, USA
[c] Gratings Inc., Albuquerque, NM 87107, USA

ARTICLE INFO

Article history:
Received 15 October 2010
Received in revised form
13 May 2011
Accepted 13 May 2011

Keywords:
Silicon solar cell
DLTS
AFORS-HET
Deep levels defects
Spin-on-doping
Light current voltage

ABSTRACT

Introduction of deep level defects during thermal diffusion of phosphorous (P) in silicon (Si) using spin-on-doping (SOD) from phosphosilicate glass (PSG) was studied using deep level transient spectroscopy (DLTS). The structure was utilized as a solar cell and defect-induced-degradation of the cell efficiency was studied and modeled. The light current–voltage (LIV) measurements performed on as-fabricated solar cell yielded open circuit voltage, short-circuit current density, fill factor (*FF*) and efficiency to be 540 mV, 24 mA/cm^2, 40% and 5%, respectively. Whilst the simulation of the similar solar cell using AFORS-HET software revealed significantly higher data than the experimental ones. However, by including three deep level defects H_1–H_3 (holes) having activation energies (eV) 0.23, 0.33 and 0.41 in the modeled solar cell, the simulated results were observed in remarkably good agreement with experimental data. Our DLTS measurements practically witnessed H_1–H_3 defect levels in p-layer of the cell.

© 2011 Elsevier B.V. All rights reserved.

1. Introduction

Presently the energy requirements are being met largely from the non-renewable energy resources especially oil and gas, thus creating environmental issues. This has spurred the world to look for alternate sources of energy like biological sources, hydropower, nuclear fission, wind energy, solar–thermal and photovoltaic (PV) [1,2]. The PV industry has shown a tremendous potential and experienced rapid growth, making solar energy an affordable option [3]. The backbone of this industry is silicon (Si) where ~90% of solar cells are being made from this material [4–6]. To reduce the cost of the solar cells boron doped Czochralski (Cz) and/or multi crystalline (mc) Si wafers are being used as starting material instead of expensive and high quality float zone (fZ) Si [7,8]. However, as-fabricated solar cells could not deliver theoretically expected efficiency i.e. ~30%, due to a number of reasons such as incomplete absorption of incident light, presence of intrinsic or processing induced defects/dislocations [9]. Maximum light absorption has been achieved using different schemes like anti-reflection coating (ARC) or surface texturing [10]. Though a number of investigations have been performed to study the properties of defects in Si solar cell but a detailed understanding is still lacking. For example, Hamadeh and Darwich [11] found hole traps with activation energy 0.37 and 0.48 eV affecting efficiency of Si solar cell, drastically. Adey et al. [12] found boron–oxygen center (E_v+0.3 eV) being responsible for the degradation of Cz–Si solar cell. Reehal et al. [13] associated iron–boron complex (E_v+0.33 eV) with the source of malfunctioning of Si-solar cells. In short, the deep level defects are known to impose detrimental effects on the efficiency of Si solar cells, thereby a detailed and comprehensive understanding is necessary to address the failure.

In this paper, generation of defects during thermal diffusion of phosphorous from PSG is reported. As a result, the influence of the deep level defects on the efficiency of Si-solar cells using experimental and simulation methods was examined for the diode structure created by the above method. The light current voltage (LIV) measurements yielded efficiency (η) of the as-fabricated Si solar cell to be ~5% as compared to 14.4% of the modeled Si-solar cell (defect free). However, on introduction of three deep level defects (hole traps) in the solar cell (modeled), the simulated LIV data were found strikingly in agreement with the experimental results. Presence of the deep level defects was confirmed by deep level transient spectroscopy (DLTS) measurements [14], where three prominent hole traps were found in the p-layer of the solar cell having activation energies 0.23, 0.33 and 0.41 eV, respectively, above the valence band edge.

2. Experimental

Boron doped p-Si (1 0 0) wafer of 1.1 Ω cm resistivity was used to fabricate the solar cell by inducing n-type layer using spin-on-dopant (SOD) technique. Resistivity was measured by the four

* Corresponding author. Tel.: +92 3017724897.
E-mail address: mhashmi@iub.edu.pk (M. Asghar).

0927-0248/$ - see front matter © 2011 Elsevier B.V. All rights reserved.
doi:10.1016/j.solmat.2011.05.032

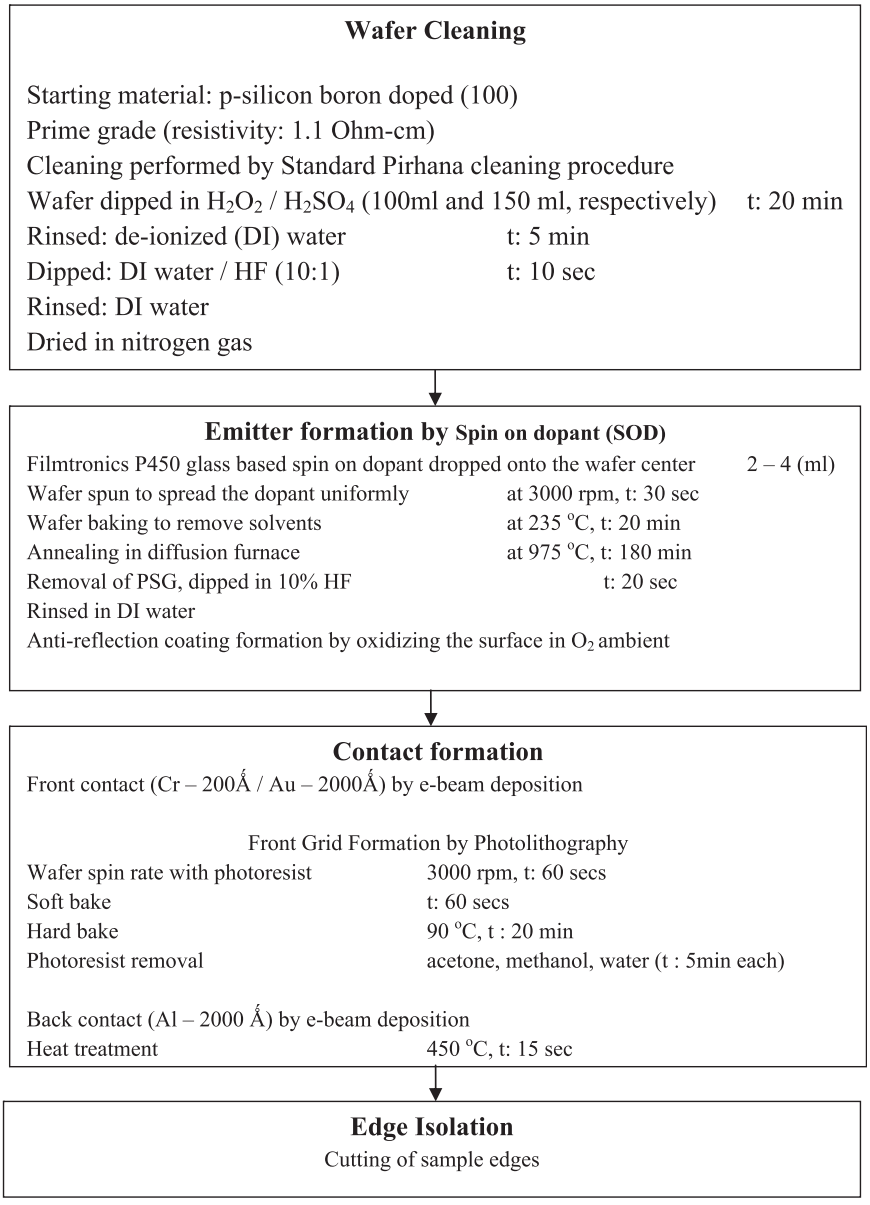

Fig. 1. An overview of the applied process sequence performed during the fabrication of silicon solar cell by spin-on-dopant technique. The basic steps are wafer cleaning, p–n junction formation by spin-on-dopant and front and back contact formation.

point probe method. The details of the fabrication process of solar cell is following (see also Fig. 1).

2.1. Cleaning

The wafer was cleaned using the standard piranha cleaning method. First, a mixture of 100 ml of H_2O_2 and 150 ml of H_2SO_4 was prepared in a beaker and the wafer was fully submersed for 20 min. This was followed by a DI water rinse until the resistivity was 12 MΩ. Later, the wafer was dipped in 10% HF for about 15 s to remove the oxide layer on the wafer followed by a DI water rinse until the resistivity was 12 MΩ.

2.2. p–n junction formation

The p–n junction was formed using two steps. First the dopant source material was deposited on the surface of the wafer and then driven into the wafer at a high temperature.

2.2.1. Deposition

Filmtronics P450, a glass based spin-on-dopant was used as the source of phosphorus dopant. P450 is a clear and viscous glass based liquid stored under controlled temperature. For preparation, the liquid is allowed to acclimate to room temperature for a minimum of 4 h. Then a few drops (from 2 to 4 ml) are placed on the center of the wafer and then spun immediately at 3000 rpm for 30 s to get a uniform coating of the spin-on-dopant. The wafer is then baked on a hot plate for 20 min at 235 °C to remove all solvents.

2.2.2. Drive-in

The prepared wafer with the phosphorus dopant on the surface is next loaded into a tube furnace to initiate diffusion of the dopant material into the wafer. The loading time into the furnace was 5 min and the wafer remained in the furnace for 180 min at 975 °C with constant oxygen flow. At the end of the 3 h, the wafer was removed and let to sit at the mouth of the furnace for 10 min

before being allowed to cool to room temperature and subsequent removal of the phosphosilicate glass (PSG). This was accomplished by a 20 s dip in 10% HF. The wafer was then rinsed in DI water until the resistivity of the water was 12 MΩ.

2.3. Contacts preparation

Contacts were prepared by e-beam deposition technique. On the emitter side, chromium of 200 Å was first deposited followed by 2000 Å of gold. Chromium was necessary to provide adhesion between silicon and the gold.

2.3.1. Front side grid

The front side grid was designed using AutoCAD and printed on a transparency sheet. Though not the best of the methods, it worked well for large features. The front side pattern was transferred to the cell using the standard photolithography and wet etching technique.

Photoresist was spun on the wafer at 3000 rpm for 60 s, followed by a 60 s soft bake. The mask was then placed on the wafer and exposed to 150 mJ/cm^2 of UV followed by a 60 s rinse in 100 ml of micro-positive 354 developer and 1 min rinse in DI water. The wafer was then hard baked in an oven at 90 °C for 20 min. Wet etching was carried out at room temperature. The gold was etched in a gold etching solution for 30 s followed by chrome etch for 5 s with a sift rinse to separate the 2 steps and removal of excess etching solution on the wafer. The wafer was then rinsed in acetone, methanol and water for 5 min each to remove the photoresist.

2.3.2. Backside contact

For the backside contact aluminum (Al) with thickness of 2000 Å was deposited using the e-beam technique. This was followed by a heat treatment in a tube furnace for 15 s at 450 °C, followed by dicing and testing.

LIV, capacitance–voltage (C–V) measurements and DLTS measurements were performed by Tektronix 370B, Boonton 7200 capacitance meter and DLS-83D spectrometer, respectively, whereas simulation was performed by one dimensional numerical simulation software AFORS-HET v 2.4.1 [15].

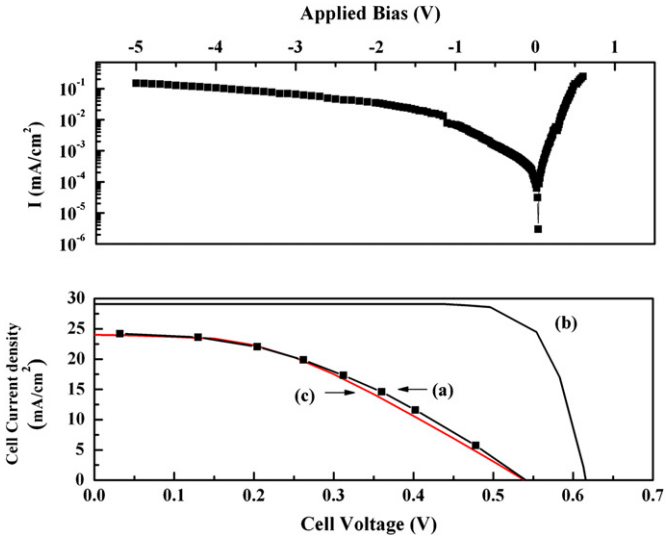

Fig. 2. Current–voltage measurements of a representative solar cell. Top: dark IV of the solar cell to evidence the low leakage current of the device; down: experimental LIV curve measured using one sun AM 1.5 (1000 W/m^2) irradiation as a reference. A theoretically generated LIV data by AFROS-HET using triple defect level simulation (TDLS) procedure, shows a fair agreement with the experimental data (curve a), which otherwise exhibits a significant difference with respect to the experimental one, if simulated for a defect free solar cell (curve b).

3. Results and discussion

Fig. 2a demonstrates dark I–V characteristics of the representative solar cell (SC) evidencing low leakage current of the device that is favorable for obtaining good efficiency of the cell. Fig. 2b displays three LIV curves corresponding to: (a) as-fabricated SC, (b) simulated defect free SC and (c) SC simulated with three hole traps. All measurements were performed/simulated using one sun AM 1.5 (1000 W/m^2) irradiation as a reference. Curve (a) significantly deviates from the simulated curve (b) yielding V_{oc} (mV), I_{sc} (mA/cm^2), FF and η to be 540, 24, 40% and 5% against 640, 29, 77% and 14.4%, respectively, detail is given in Table 1. To justify the discrepancy, we re-designed the solar cell by sequentially incorporating hole trap(s) in three groups referred as single defect level simulation (SDLS: E_v+0.23 eV), double defect level

Table 1
List of parameters incorporated for the simulation of solar cell performance fingerprints (V_{oc}, I_{sc}, FF and η). Column II of the table describes the associated parameters of deep level defects used for SDLS/DDLS/TDLS procedures.

Phosphorus diffused region (emitter)	Anti-reflection coating (AR): 80 nm SiO_2 Doping density: 4×10^{19} cm^{-3} Front surface recombination velocity: 1×10^5 cm/s Junction depth: 2 μm	
Base	Doping density: 1.68×10^{15} cm^{-3} Base thickness 450 μm Defect free	H_1: trap energy=0.23 eV Capture cross-section=1.94×10^{-16} cm^2 Trap concentration=7×10^{11} cm^{-3} H_2: trap energy=0.33 eV Capture cross-section=1.65×10^{-16} cm^2 Trap concentration=2.5×10^{12} cm^{-3} H_3: trap energy=0.41 eV Capture cross-section=7.2×10^{-18} cm^2 Trap concentration=4.5×10^{12} cm^{-3}
Back surface field	Doping density=1×10^{18} cm^{-3} Back surface recombination velocity=1×10^5 cm/s Junction depth=0.1 μm	

simulation (DDLS: $E_v+0.23$ eV, $E_v+0.33$ eV) and triple defect level simulation (TDLS: $E_v+0.23$ eV, $E_v+0.33$ eV, $E_v+0.41$ eV). As a result, the simulated data for TDLS i.e. curve (c) was found in a fair agreement with the experimental data i.e. curve (a). In order to justify the three traps model of solar cell we performed DLTS measurements. Fig. 3 shows the DLTS spectrum of the investigated solar cell, measurement conditions are inserted therein. Three hole trap levels were observed in the DLTS spectrum namely H_1, H_2 and H_3 at 155, 209 and 307 K, respectively. Electronic fingerprints of the deep level defects (from H_1 to H_3) such as activation energies (E_T) and capture cross-section (σ_p) were extracted from Arrhenius plot (see Fig. 4) using Eq. (1) [16].

$$\ln(e_n/T^2)=\ln(\gamma\sigma_p)-E_T/kT \quad (1)$$

where e_n (emission rate (s^{-1})), T (peak temperature (K)), γ (pre-exponential factor: 1.78×10^{21} s^{-1} cm^{-2} for p-Si (active layer)), σ_p (hole capture cross-section (cm^2)) and E_T (trap energy (eV)). Trap

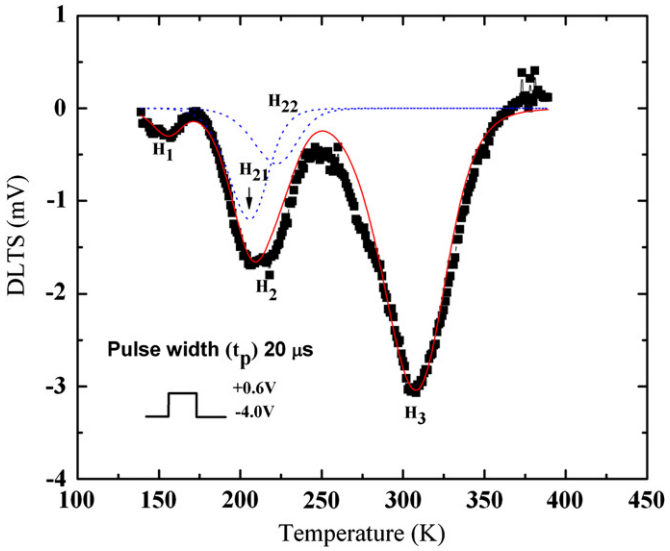

Fig. 3. A representative DLTS spectrum due to the solar cell indicates the presence of three (H_1–H_3) deep level hole defects (squares). The applied biasing and pulsing conditions maintaining rate window 217 s^{-1}, are depicted in the figure. Line shape analysis (lines and dots) reveals a doublet nature of H_2 level to be (H_{21} and H_{22}).

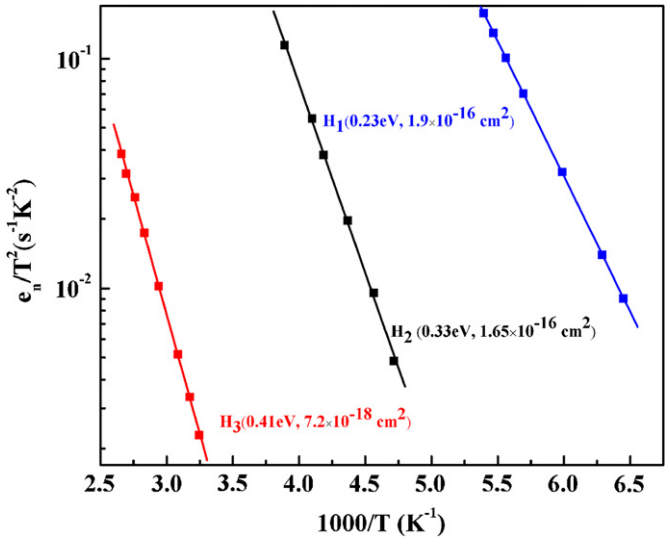

Fig. 4. Arrhenius plots of the H_1–H_3 trap levels observed in p-Si layer of the solar cell. The electrical parameters such as activation energy and capture cross-section of the defect levels are inserted therein.

concentration (N_T) was worked out from Eq. (2)

$$N_T=2N_D\Delta C/C_o \quad (2)$$

here, $\Delta C/C_o$ (maximum DLTS signal for the particular peak), N_A (doping concentration of the p-Si (active layer)). N_A was calculated from C–V measurement and found to be 2×10^{15} cm^{-3}, which is consistent with the resistivity of the wafer. For H_1, H_2 and H_3, E_T were found to be 0.23, 033 and 0.41 eV, respectively, σ_p was equal to, 1.9×10^{-16}, 1.65×10^{-16} and 7.2×10^{-18} cm^2, respectively, and N_T was 7×10^{11}, 2.5×10^{12} and 4.5×10^{12} cm^{-3}, respectively. In order to ascertain whether these defects were already present in the starting material/substrate, we also performed DLTS measurements on virgin (untreated) substrate (p-Si) but could not observe any traps therein.

Theoretical line shape analysis of the DLTS spectrum is a useful tool to check the singlet and/or doublet nature (if any) of the observed deep level defects. The description of the line shape Eq. (3) is given in the following [17]:

$$A(y)=2\pi(1-e^{-y})/(4\pi^2+y^2) \quad (3)$$

where $A(y)$ is the amplitude of peak, $y=t/\tau$; $t=1/f$ and $\tau=1/e_n$ where 't' time period, 'f' lock-in-frequency, 'τ' time constant and 'e_n' is the emission rate. Line shape analysis reveals that H_2 level has a doublet nature consisting of two hole traps H_{21} and H_{22} at 206 and 222 K, respectively. The activation energies of these levels (H_{21} and H_{22}) were estimated to be 0.31 eV and 0.32 eV, respectively.

3.1. Deep level defects

Table 3 enlists significant deep level defects in Si based solar cells reported so far. The associated information reveals that divacancy, iron–boron, iron–oxygen, carbon–vacancy and carbon–oxygen are commonly induced deep level defects in the solar cells. Essential sources of these defects are irradiation, implantation and/or heat treatment especially for doping purposes [18–20]. Briefly, heat treatment creates Si vacancies by Si out-diffusion mechanism, and subsequently the electrically inactive residual carbon (whose major source is crucible), boron and/or oxygen contents occupying interstitial/dislocation sites in Si wafer form active complexes with vacancies such as divacancy, oxygen–vacancy (O–V) and boron–vacancy (B–O) and/or carbon–vacancy–oxygen (C–V–O) [21–24]. A careful look of the data given in Table 3, indicates that

Table 2
List of various parameters of the modeled solar cell (Si) extracted from application of SDLS, DDLS and TDLS procedures. DDLS procedure shows that the presence of H_2 level in combination of H_1 or H_3 decreases the efficiency of solar cell by ~27% or ~29%, respectively. Whereas the SDLS method indicates that level H_2 has adverse effect in comparison to the H_1 and H_3, altogether. Finally TDLS procedure fits well with the experimental curve, which exhibits ~5% efficiency as compared to defect free solar cell i.e. 14.4%. Last column represents the efficiency loss with respect to the efficiency of defect free solar cell.

Defect(s)	V_{oc} (mV)	I_{sc} (mA/cm^2)	FF (%)	η (%)	Impurity-effective efficiency loss with respect to 14.4%
Single defect level simulation (SDLS) procedure					
H_1	595.7	28.12	76.08	12.74	11.5
H_2	548	25.51	76.08	10.63	26.2
H_3	610.5	26.39	77.23	12.44	13.6
Double defect level simulation (DDLS) procedure					
H_1–H_2	544.1	25.38	76.3	10.54	26.8
H_2–H_3	544.9	24.78	75.85	10.24	28.9
H_1–H_3	589	26.07	73.57	11.3	21.5
Triple defect levels simulation (TDLS) procedure					
H_1–H_2–H_3	540	24	40	5	65.3

Table 3
A brief literature review of deep level defects observed in Si solar cells with the help of DLTS technique is tabulated. Possible source and origin of these defects are also listed therein.

References	Activation energy (eV)	Source/origin of defects	Identification of defects
Abdelbarey [32]	$E_v+0.39$ $E_v+0.10$ $E_v+0.33$ $E_v+0.20$	Intentional iron contaminated	Fe–B Fe_i iron related defect
Reehal et al. [13]	$E_v+0.33$ $E_c-0.53$	Un-intentional iron induced in solar cell processing	Fe–O complex Fe–B complex
Schmidt and Cuevas [28]	$E_v+0.35$ E_c–0.45	Cz silicon growth and illumination induced defects	B–O complex
Das et al. [18]	$E_v+0.15$ $E_v+0.17$ $E_v+0.23$ $E_v+0.32$ $E_v+0.33$ $E_v+0.54$ $E_v+0.60$	Electron beam deposition Proton and electron irradiation	Irradiation induced and divacancy
Capan et al. [33]	$E_v+0.33$ $E_v+0.39$	Carbon implant iron doped	Dislocation with clouds of carbon/metallic impurities
Hamadeh and Darwich [11]	$E_v+0.38$ $E_v+0.48$	Manufacturing, technological and processing steps	Fe_i iron defect complex
Adey et al. [12] Asghar et al. [19]	$E_v+0.30$ $E_v+0.23$ $E_v+0.41$	Oxygen and boron doping in Cz silicon growth Alpha irradiation	B–O meta-stable defect Divacancy C–V–O complex
This study	$E_v+0.23$ $E_v+0.33$ $E_v+0.41$	Solar cell processing (thermal treatments)	Divacancy B–O C–V–O complex

activation energies corresponding to divacancy, B–O and C–V–O are 0.23 ± 0.02, 0.33 ± 0.02 and 0.4 ± 0.02, respectively. In this perception, we correlate the observed hole traps (H_1, H_2 and H_3) with divacancy, B–O and C–V–O complexes, respectively, detail is given in the following.

3.2. Influence of traps on the performance of silicon solar cell

The hole trap H_1 at 0.23 eV is a well known divacancy [25,26]. Divacancy is supposed to capture two holes from the p-layer and thereby leaves two electrons unpaired in n-layer of the solar cell. Using the defect-free solar cell, which exhibits 14.4% efficiency, as a reference, we have estimated influence of the observed deep level defects (one by one) on the efficiency of the fabricated solar cell from the diode using SDLS procedure. The details are shown in Table 2. In this perception, H_1 level has been found to decrease the efficiency of the device from the reference of 14.4–12.74%. A doublet level H_2 (H_{21}: 0.3 and H_{22}: 0.33 eV) is associated with the meta-stable B–O defect [27,28]. It is commonly known as one of the most effective recombination centers and minority carrier lifetime killer. It therefore, affects the performance of Si solar cell at a large scale. The SDSL procedure also supports this argument i.e. the loss is $\sim$26% compared to the reference simulated efficiency (14.4%) of the modeled Si solar cell, which brings the efficiency down to 10.63%. The hole trap H_3 having activation energy $\sim$0.41 eV is related to carbon–vacancy–oxygen complex (C–V–O) [29,30]. Some reports however, relate the level having nearly similar features of H_3 level to iron–boron and/or iron–oxygen complex in iron doped Si. Since the investigated samples were boron doped, therefore we do not attribute our H_3 level with iron and/or iron–boron complex [23,31]. In fact, C and O are generally known as residual defects occupying interstitial and/or dislocation sites in Si wafer, therefore correlation of H_3 level with C–V–O seems plausible (explained earlier). From SDLS procedure, this level is found to impose $\sim$14% loss of the efficiency of the reference Si solar cell (defect free). The comparison shows that level H_2 has the highest detrimental effect on the efficiency of crystalline silicon solar cell i.e. it inflicts $\sim$26% efficiency loss compared to that of (14.4%) a defect free solar cell. Similarly the losses in efficiencies with respect to various combinations of defects using DDLS and TDLS procedures are depicted in Table 2. Where from H_1 to H_3 defect levels altogether in p-Si, degrade about 66% efficiency of the solar cell and thereby, the cell exhibits only 5% efficiency, which is in a remarkable good agreement with our experimental results.

4. Conclusion

In this study, generation of deep level defects during thermal diffusion of phosphorous from PSG was studied using DLTS. Consequently, the influence of deep level defects on the performance of crystalline silicon solar cells from the same material was investigated using experimental and simulation methods. From LIV measurements V_{oc}, I_{sc}, FF and η were found to be 540 mV, 24 mA/cm^2, 40% and 5% with respect to simulated values: 614 mV, 29 mA/cm^2, 77% and 14.4%. From SDLS method, we came to know that defect level H_2 at $E_v+0.33$ eV had the adverse effect (26% loss of efficiency with respect 14.4%) on the performance of Si solar cell. Eventually, when all deep levels were incorporated in the simulation program, both the theoretical and the experimental data were in agreement. The results were also confirmed by our DLTS measurements, which revealed three hole traps (H_1–H_3) at 0.23, 0.33 and 0.41 eV in the p-layer of the cell, respectively. Amongst them 0.23 eV was identified as a divacancy, 0.33 eV was related to the meta-stable boron–oxygen complex and 0.41 was identified as carbon–vacancy–oxygen complex. Interestingly, H_2 was found to be an efficient recombination center and minority carrier lifetime killer.

Acknowledgments

Authors are grateful to HEC—Pakistan under 1019/R&D/2007, USEF—Pakistan and Fulbright USA for financial support to carry out this research activity.

References

[1] R.C. Neville, Solar Energy Conversion: The Solar Cell, Energy needs-Energy sources, 2nd Ed., Elsevier, Amsterdam, 1995, pp. 1–38.
[2] A. Bentzen, Phosphorous Diffusion and Gettering in Silicon Solar Cells, Ph.D. Thesis, University of Oslo, Amsterdam, 2006 p. 1.
[3] A.G. Aberle, Fabrication and characterization of crystalline silicon thin-film materials for solar cells, Thin Solid Films 511 (2006) 26–34.
[4] D.H. Neuhaus, A. Münzer, Industrial silicon wafer solar cells, Advances in OptoElectronics (2007) 1–15 Article ID 24521.
[5] J.Y. Lee, Rapid Thermal Processing of Silicon Solar Cells—Passivation and Diffusion, Ph.D. Thesis, Fraunhofer Institut fur Solare Energiesysteme (ISE), Amsterdam, 2003, p. 1.
[6] M.A. Green, Crystalline silicon photovoltaic cells, Advanced Materials 13 (2001) 1019–1022.
[7] F. Aratani, The present status and future direction of technology development for photovoltaic power generation in Japan, Progress in Photovoltaics: Research and Applications 13 (2005) 463–470.
[8] K. Nakayashiki, Understanding of Defect Passivation and its Effect on Multi-crystalline Silicon Solar Cell Performance, Ph.D. Thesis, Georgia Institute of Technology, GA, USA, 2007, p. 3.
[9] A. Goetzberger, C. Hebling, H.W. Schock, Photovoltaic materials, history, status and outlook, Material Science Engineering R 40 (2003) 1–46.
[10] M.L. Kuo, D.J. Poxson, Y.S. Kim, F.W. Mont, J.K. Kim, E.F. Schubert, S.Y. Lin, Realization of near-perfect antireflection coating for silicon solar energy, Optics Letters 33 (2008) 2527–2529.
[11] H. Hamadeh, R. Darwich, DLTS properties of iron defects in crystalline silicon used in solar cells, Material Science Engineering B 113 (2004) 166–169.
[12] J. Adey, R. Jones, D.W. Palmer, P.R. Briddon, S. Öberg, Degradation of boron-doped Czochralski-grown silicon solar cells, Physical Review Letters 93 (2004) 055504–055508.
[13] H.S. Reehal, M.P. Lesniak, A.E. Hughes, Application of DLTS to silicon solar cell processing, Journal of Physics D: Applied Physics 29 (1996) 934–938.
[14] D.V. Lang, Deep-level transient spectroscopy: a new method to characterize traps in semiconductors, Journal of Applied Physics 45 (1974) 3023–3032.
[15] A. Froitzheim, R. Stangl, L. Elstner, M. Kriegel, W. Fuhs, AFORS-HET: a computer-program for the simulation of heterojunction solar cells to be distributed for public use, in: Proceedings of Third World Conference on Photovoltaic Energy Conversion, IEEE, Osaka, Japan, B 2003, pp. 279–282.
[16] D.K. Schroder, Semiconductor Material and Device Characterization, Defects, 3rd Ed., Wiley, NewYork, 2006 (p. 262).
[17] D.V. Lang, Thermally Stimulated Relaxation in Solids, Space-charge spectroscopy in semiconductors, vol. 37, Springer, NewYork, 1979 (p. 113).
[18] A.G.M. Das, C. Nyamhere, F.D. Auret, M. Hayes, A comparative study of electronic properties of the defects introduced in p-Si: (i) during electron beam deposition of Ti/Mo, (ii) by proton irradiation, and (iii) by electron irradiation, Surface and Coatings Technology 203 (2009) 2628–2631.
[19] M. Asghar, M. Zafar Iqbal, N. Zafar, Study of alpha-radiation-induced deep levels in p-type silicon, Journal of Applied Physics 73 (1993) 4240–4247.
[20] P.K. Giri, Y.N. Mohapatra, Thermal stability of defect complexes due to high dose MeV implantation in silicon, Material Science Engineering B 71 (2000) 327–332.
[21] P.J. Ribeyron, F. Durand, Oxygen and carbon transfer during solidification of semiconductor grade silicon in different processes, Journal of Crystal Growth 210 (2000) 541–553.
[22] A.R. Peaker, J.H. Evans-Freeman, P.Y.Y. Kan, I.D. Hawkins, J. Terry, C. Jeynes, L. Rubaldo, Vacancy-related defects in ion implanted and electron irradiated silicon, Material Science Engineering B 71 (2000) 143–147.
[23] Vikash Dubey, Shyam Singh, Role of oxygen and carbon on donor formation in step-annealed CZ-silicon, Journal of Physics and Chemistry of Solids 65 (2004) 1265–1269.
[24] J.D. Gerson, L.J. Cheng, J.W. Corbett, A quenched-in defect in boron-doped silicon, Journal of Applied Physics 48 (1977) 4821–4822.
[25] M. Mamor, M. Willander, F.D. Auret, W. Meyer, E. Sveinbjornsson, Configurationally metastable defects in irradiated epitaxially grown boron-doped p-type Si, Physical Review B 63 (2000) 045201–045205.
[26] F. Volpi, A.R. Peaker, I. Berbezier, A. Ronda, Electrically active defects induced by sputtering deposition on silicon: the role of hydrogen, Journal of Applied Physics 95 (1994) 4752–4760.
[27] J. Schmidt, A.G. Aberle, R. Hezel, Investigation of carrier lifetime instabilities in Czochralski silicon, in: Proceedings of 26th IEEE PVSC, IEEE, Anaheim, California, USA, vol. 26, 1997, pp. 13–18.
[28] J. Schmidt, A. Cuevas, Electronic properties of light-induced recombination centers in boron-doped Czochralski silicon, Journal of Applied Physics 86 (1999) 3175–3180.
[29] P.M. Mooney, L.J. Cheng, M. Suüli, J.D. Gerson, J.W. Corbett, Defect energy levels in boron-doped silicon irradiated with 1-MeV electrons, Physical Review B 15 (1977) 3836–3843.
[30] B. Pivac, I. Kovačević, V. Borjanović, Defects in carbon and oxygen implanted p-type silicon, Nuclear Instruments and Methods in Physics Research B 186 (2002) 355–359.
[31] M. Trushin, O. Vyvenko, W. Seifert, G. Jia, M. Kittler, Iron–oxygen interaction in silicon: a combined XBIC/XRF-EBIC-DLTS study of precipitation and complex building, Physica B 404 (2009) 4645–4648.
[32] D. Abdelbarey, V. Kveder, W. Schröter, M. Seibt, Light induced point defects reactions of residual iron in crystalline silicon after aluminum gettering, Journal of Applied Physics 108 (2010) 043519–043524.
[33] I. Capan, V. Borjanovic, B. Pivac, Dislocation-related deep levels in carbon rich p-type polycrystalline silicon, Solar Energy Materials and Solar Cells 91 (2007) 931–937.